

RESEARCH

Open Access



# Surface display of eugenol oxidase and dioxygenase complex as a sustainable biocatalyst for efficient bioconversion of lignin-derived 4-n-propylguaiacol to vanillin

Yongqing Tian<sup>1</sup>, Yige Yang<sup>1</sup>, Minmin Ni<sup>2</sup> and Jing Wo<sup>1\*</sup>

## Abstract

**Background** Vanillin is a widely utilized flavor compound of significant value in the food and pharmaceutical sectors, which can be obtained through natural extraction, chemical synthesis, or biotechnological processes. However, the yield from vanilla pods is insufficient to meet market demand, and chemically synthesized vanillin not only encounters limitations in its application within the food and pharmaceutical industries but also needs to address environmental concerns and unsustainable raw material sources. Hence, it is imperative to explore alternative approaches to develop an efficient and cost-effective green vanillin. To address the challenges encountered in vanillin biosynthesis, such as substrate uptake limitations and product-induced inhibition of cell growth, we leveraged the advantages of surface display technology and artificial multi-enzyme scaffolds to construct a hybrid surface-display biocatalytic system by assembling Eugenol oxidase (EUGO) and dioxygenase (NOV1), which can convert lignin biowaste 4-n-propylguaiacol (4-PG) into vanillin on the surface of *Escherichia coli* BL21(DE3).

**Results** To assemble bioactive macromolecules of EUGO and NOV1 on the surface of *E. coli* BL21(DE3), we utilized Lpp-OmpA-SpyCatcher (LOAS) as an anchoring motif and displayed EUGO-linker-NOV1-SpyTag (ELNS) by covalent interaction between SpyTag and SpyCatcher to allow their spatial proximity. After optimization of the reaction system, our self-assembly display system exhibited highly efficiency in converting 4-PG into vanillin and reached a final concentration of vanillin at 12.58 g/L, 2.5 times higher than that achieved by the whole-cell biocatalytic system. The LOAS-ELNS display system was applied to the sustainable biosynthesis of vanillin from lignin-derived 4-n-propylguaiacol at least 10 times.

**Conclusions** This work provided a generalized approach to co-expressing proteins and offered an efficient, eco-friendly, and renewable method for the biosynthesis of vanillin from 4-PG.

**Keywords** Vanillin, Surface display, Eugenol oxidase, SpyCatcher-SpyTag, Whole-cell biocatalyst

\*Correspondence:

Jing Wo

wojing0330@zjut.edu.cn

<sup>1</sup>Institute of Engineering Biology and Health, Collaborative Innovation Center of Yangtze River Delta Region Green Pharmaceuticals, College of

Pharmaceutical Sciences, Zhejiang University of Technology, Hangzhou 310014, China

<sup>2</sup>Jiangsu Key Laboratory of Advanced Catalytic Materials and Technology, School of Petrochemical Engineering, Changzhou University, Changzhou 213164, China



© The Author(s) 2025. **Open Access** This article is licensed under a Creative Commons Attribution-NonCommercial-NoDerivatives 4.0 International License, which permits any non-commercial use, sharing, distribution and reproduction in any medium or format, as long as you give appropriate credit to the original author(s) and the source, provide a link to the Creative Commons licence, and indicate if you modified the licensed material. You do not have permission under this licence to share adapted material derived from this article or parts of it. The images or other third party material in this article are included in the article's Creative Commons licence, unless indicated otherwise in a credit line to the material. If material is not included in the article's Creative Commons licence and your intended use is not permitted by statutory regulation or exceeds the permitted use, you will need to obtain permission directly from the copyright holder. To view a copy of this licence, visit <http://creativecommons.org/licenses/by-nc-nd/4.0/>.

## Background

Natural vanillin (4-hydroxy-3-methoxybenzaldehyde, C<sub>8</sub>H<sub>8</sub>O<sub>3</sub>), known as the “queen of flavors,” is extracted from vanilla pods and possesses exceptional chemical properties that make it highly advantageous in various industries including chemical, pharmaceutical, agriculture, tobacco, and cosmetics [1, 2]. Moreover, it is also used as a biological preservative due to its antibacterial, anti-mutagenic, and antioxidant properties [3]. Owing to the low yields in the supply of natural vanillin, high production and maintenance expenses, and the specific climatic conditions required for cultivating vanilla plants, vanillin derived from plant sources constitutes less than 1% of the global market share [4]. Another important commercial method is chemical synthesis, the predominant substrates of which are isoeugenol and phenol, and the process usually involves multi-step chemical reactions such as oxidation, decarboxylation, and acidification [4]. Although chemical synthesis of vanillin offers lower costs and higher yields compared to traditional extraction methods, it is declining in interest in the food industry for its adverse impacts on the environment and human health [4, 5]. Hence, the increasing demand for sustainable and natural vanillin has prompted the exploration of alternative, cost-effective and bio-based methods.

According to the report, the global market for bio-based vanillin was valued at approximately 216.78 million USD in 2021 and is forecasted to grow at a compounded annual growth rate of 6.98%, reaching an estimated value of 326.24 million USD by 2027 [6]. To meet the growing demand for bio-based vanillin, various bio-based approaches have been reported in the literature, such as plant cell culture techniques, microbial fermentation, and bioconversion techniques [7–10]. Some natural microorganisms exhibit the ability to synthesize vanillin in low quantities. However, these processes encounter multiple challenges, such as low conversion efficiency, rapid degradation rates, and the cytotoxicity of the product, which restrict their applicability in large-scale production [3]. Researchers have increasingly turned to microbial fermentation to biotransform various raw materials, such as ferulic acid, isoeugenol, and feruloyl coenzyme A (CoA), into vanillin [11]. The construction of biosynthetic pathways using sequential enzymes is an effective approach for synthesizing target molecules, whether these pathways exist naturally or are artificially engineered [12, 13]. In 1998, recombinant *E. coli* was constructed to introduce a *de novo* biosynthetic pathway of vanillin based on the naturally occurring vanilla pathways in plants, resulting in only trace amounts of detectable vanillin [14]. After that, a variety of biosynthetic pathways and strategies have been employed to produce vanillin in diverse microorganisms [15]. However, these biosynthetic

systems also have their own limitations that prevent them from achieving satisfactory productivity levels. For example, the growth of *Pediococcus acidilactici* M16 is inhibited when the vanillin concentration reaches 9–10 g/L [16]. Similarly, *Saccharomyces cerevisiae* exhibits inhibited growth at vanillin concentrations exceeding 0.5–1 g/L [17]. Except for the aforementioned methods, the bioconversion technique avoids the formation of byproducts and prevents cytotoxicity caused by the substrate or vanillin. Recently, an eugenol oxidase was utilized for the enzymatic synthesis of vanillin through the oxidation of vanillyl alcohol, achieving a yield of 2.9 g/L/h [18]. Subsequently, by immobilizing the eugenol oxidase and optimizing the reaction conditions, the vanillin yield was significantly enhanced to 9.9 g/L/h [19]. In another study, Kim et al. developed a one-pot enzymatic conversion process for transforming capsaicinoids into vanillin by retracing the biosynthetic pathway identified in *Capsicum* plants [20]. The enzyme cascade, involving sequential actions by immobilized lipase B from *Candida antarctica* for the hydrolysis of capsaicinoids and  $\omega$ -transaminase from *Paracoccus denitrificans* for the oxidative deamination of the resulting vanillylamine, achieves a reaction yield of vanillin from capsaicinoids exceeding 95% in a one-pot cascade reaction. This process effectively prevents the undesirable accumulation of oxidation byproducts and inhibitory intermediates, specifically vanillic acid, and vanillylamine [20]. Similarly, the bioconversion technique has its own limits. For cell-based systems, intermediate or products inhibition may occur; the cell membrane acts as a barrier for substrate transportation and is more likely to generate undesirable metabolic by-products that may be toxic to cells and difficult to separate; additionally, enzymes are sometimes insoluble [20, 21]. For cell-free systems, enzymes are not only vulnerable to organic solvents, extreme temperatures, and pH values but also require the addition of necessary cofactors to perform their functions [22].

Surface display technology has been extensively utilized in the manufacturing of various chemical products, such as Pregnenolone, 15 $\beta$ -OH-deoxycorticosterone, Polyhydroxybutyrate, lactate, and succinate [23]. However, to date, there appears to be a lack of literature documenting the application of this technology in vanillin production. By anchoring a target protein to the outer membrane of a cell, cell surface display not only preserves the bioactivity of enzymes but also enhances their stability and reusability, thereby circumventing the intricate processes of cellular lysis or protein purification [24]. Moreover, co-displaying enzymes can further enhance the catalytic efficiency in multi-enzyme biosynthetic steps by reducing the spatial distance between enzymes through enzyme fusion using a short flexible peptide linker or enzyme–enzyme ligation via a covalent peptide

interaction [25]. The Lpp-OmpA, a well-established anchoring motif for *E. coli* surface display, consists of the transmembrane domain (amino acids 46–159) derived from outer membrane protein A (OmpA), in conjunction with the signal peptide and the first 9 N-terminal amino acids of the *E. coli* lipoprotein (Lpp) [26–28]. However, similar to other anchoring motifs, the application of this approach is limited by the properties and sizes of target proteins [29]. The SpyCatcher/SpyTag toolbox has emerged as a pivotal tool for multi-enzyme applications, derived from the CnaB2 structural domain. It exhibits the remarkable capability to form stable isopeptide bonds under diverse conditions, wherein the Lys on SpyCatcher and the Asp on SpyTag can spontaneously engage in covalent interactions [30]. We are motivated to explore more efficient synthesis processes to obtain higher yields of vanillin. Here, in order to construct a highly efficient vanillin bioconversion system, the membrane anchor (Lpp-OmpA) was expressed with a SpyCatcher, while the passengers (eugenol oxidase (EUGO) from *Rhodococcus jostii* RHA1 and dioxygenase (NOV1) from *Novosphingobium aromaticivorans* DSM 12444) were furnished with the matching SpyTag binding unit [31, 32]. Both parts are expressed from separate plasmids and subsequently undergo post-translational assembly via a specific, covalent SpyCatcher/SpyTag interaction. The resultant complex is ultimately integrated into the *E. coli* cell envelope through the membrane anchor (Lpp-OmpA). With the engineered LOAS-ELNS hybrid biocatalysts, the concentration of vanillin exceeded 12.58 g/L. And this biocatalyst was reused more than 10 times, with each reuse resulting in the yield of vanillin above 9.0 g/L. This work provides a promising strategy to improve the biosynthesis of vanillin from 4-PG.

## Results and discussion

### Evaluation the performance of the co-display system by utilization of mCherry and GFP

To enhance display efficiency, we genetically fused the Lpp-OmpA (LOA) with SpyCatcher as an endogenous anchoring motif, while utilizing SpyTag to fuse passenger proteins. To assess the functionality of the hybrid system, the *sfgfp* gene, the *lpp-ompA* fragment and *spy-catcher* were cloned into pBAD24 containing an ampicillin resistance gene and *araB* promoter (named pWJ005), while the *mcherry* gene and the *spyttag* fragment were ligated into pET28a (+) with a kanamycin resistance gene and an IPTG inducible T7 promoter (named pWJ006). The constructed design was presented in Fig. 1A and B. Given that the LPP-OmpA-sfGFP-SpyCatcher structure contains signal peptide sequences while the mCherry-SpyTag lacks such peptides, they need to form covalent bond complexes between SpyTag and SpyCatcher and subsequently be transported to the cell surface. When *E.*

*coli* BL21 (DE3) harboring plasmids pWJ005 and pWJ006 were induced with 0.4 mM IPTG and 1.0 mM arabinose, mCherry-SpyTag was observed to translocate to the cell surface following covalent binding to Lpp-OmpA-sfGFP-SpyCatcher. In contrast, when only 0.4 mM IPTG was used to induce *E. coli* BL21 (DE3) harboring plasmids pWJ005 and pWJ006, only red fluorescence was detected. The confocal fluorescence microscopy image revealed successful detection of the sfGFP and mCherry fluorescence signals in the cell envelope on Lpp-OmpA-sfGFP-SpyCatcher and mCherry-SpyTag displaying cells, respectively. The findings are consistent with our anticipated results. To demonstrate that Lpp-OmpA-sfGFP-SpyCatcher can be effectively displayed on the cell surface, we designed a human rhinovirus (HRV) 3 C protease recognition site between Lpp-OmpA and sfGFP-SpyCatcher. Human rhinovirus (HRV) 3 C protease recognizes the sequence LEVLFQGP and cleaves precisely between the residues Q and G. The Lpp-OmpA-sfGFP-SpyCatcher expression plasmid pWJ005 was transformed into BL21(DE3) cells. Following induction, the cells were harvested and resuspended. Subsequently, the resuspended cells were treated with HRV 3 C protease. The results demonstrated that treatment with the protease led to a significant 3.1-fold increase in fluorescence in the supernatant containing the digested protein fragment (sfGFP-SpyCatcher) compared to the untreated sample (Fig. S3). This result revealed that GFP was successfully decorated in the outer regions of *E. coli* BL21(DE3). Combined with the results of confocal fluorescence microscopy image analysis, it is shown that mCherry-SpyTag and Lpp-OmpA-sfGFP-SpyCatcher formed a complex by a covalent bond, followed by translocation to the cell surface (Fig. S4). In summary, we successfully constructed a co-display platform utilizing the Lpp-OmpA-SpyCatcher and SpyTag toolbox.

### Construction of EUGO and NOV1 co-display system on *E. coli* BL21(DE3) cells

The enzyme EUGO from *Rhodococcus jostii* RHA1, which harbors a covalently bound flavin adenine dinucleotide (FAD), has been extensively investigated due to its exceptional expression in *E. coli* and its ability to utilize various 4-substituted phenols as substrates [33]. Moreover, the remarkable solvent tolerance of EUGO adds to its attractiveness; for instance, it has been demonstrated that the enzyme can withstand up to 10% (v/v) dimethyl sulfoxide (DMSO) [34]. This feature makes it particularly appealing when working with poorly soluble compounds in aqueous media, such as 4-n-propylguaicol. The non-heme iron-dependent dioxygenase NOV1 from *Novosphingobium aromaticivorans* DSM 12,444 exhibits the ability to convert lignin-derived compounds, such as ferulic acid or isoeugenol, into vanillin without the

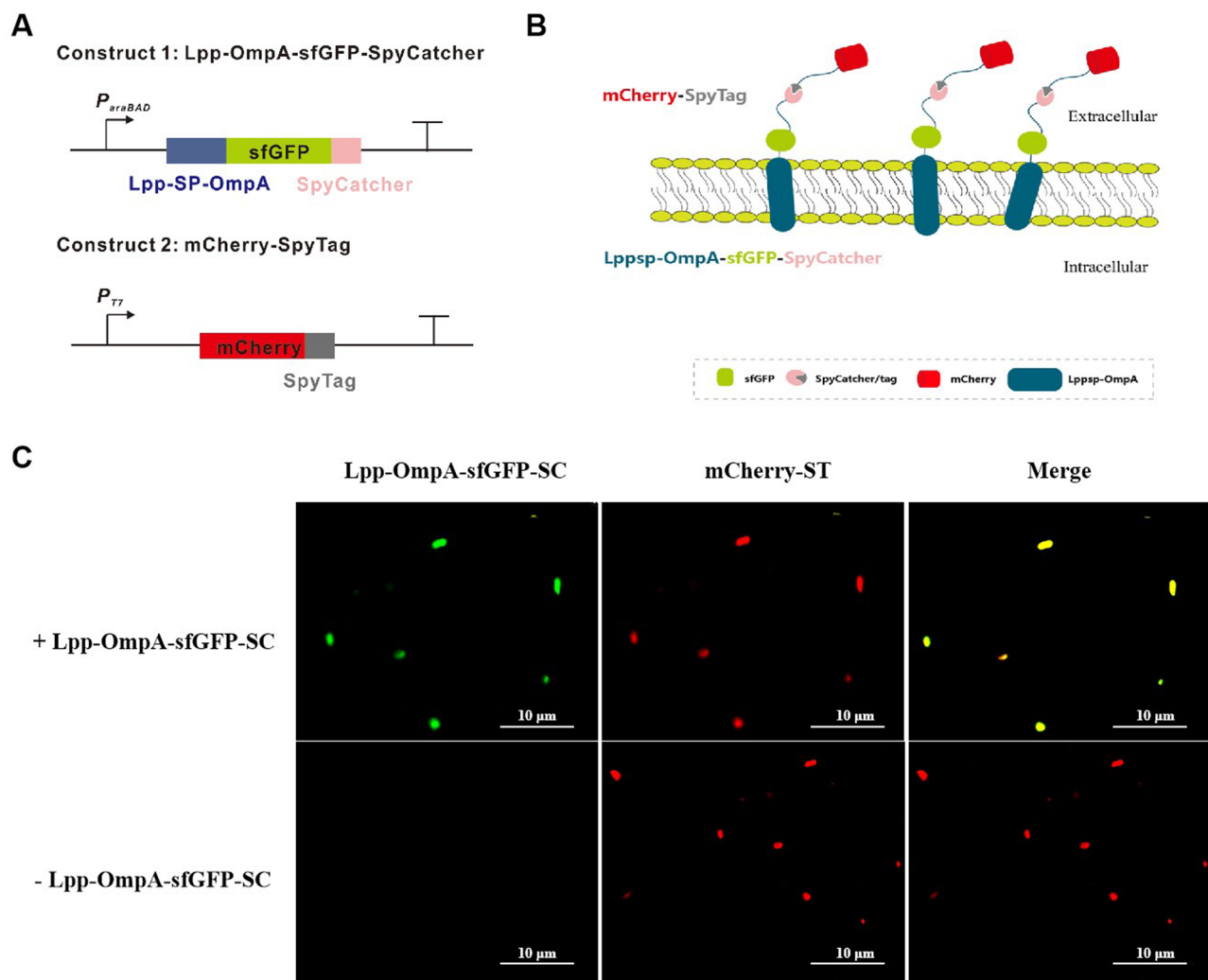


**Fig. 1** The interaction between mCherry-SpyTag and Lpp-OmpA-sfGFP-SpyCatcher and the translocation of Lpp-OmpA-sfGFP-SpyCatcher-SpyTag-mCherry to the out membrane of *E. coli* BL21(DE3). **(A)** Design of constructs for the expression of sfGFP and mCherry. **(B)** Schematic diagram demonstrated the assembly of hybrid sfGFP and mCherry complex. *E. coli* harboring plasmids pBAD24-mCherry-SpyTag and pET28a (+)-Lpp-OmpA-sfGFP-SpyCatcher were induced with L-arabinose (1.0 mM) and IPTG (0.4 mM) for translocation of mCherry-SpyTag to the cell surface after covalent interaction with Lpp-OmpA-sfGFP-SpyCatcher. **(C)** Confocal fluorescence microscopy analysis of sfGFP and mCherry after induction. Scale bars in magnified insets correspond to 10  $\mu\text{m}$

requirement for expensive cofactors. This characteristic has gained considerable interest due to its potential implications in catalysis [35].

On the one hand, the codon optimized EUGO (GenBank: ABG95085.1, 1578 bp) and NOV1 (GenBank: ABD25247.1, 1482 bp) were ligated to expression vectors pBAD24 and pET28a (+) by homologous recombination respectively, then we got two protein expression vectors pWJ001 and pWJ002. Subsequently, the plasmids were transformed into *E. coli* BL21(DE3) cells, followed by induction with 1 mM L-arabinose and 0.4 mM IPTG for protein expression. The harvested cells were lysed, and the target proteins were purified using a His-tag affinity purification system. SDS-PAGE analysis confirmed the presence of two bands at approximately 58 kDa and

55 kDa (Fig. 2C), which corresponded well with the predicted molecular weights of EUGO (57.7 kDa) and NOV1 (54.7 kDa). To validate the enzymatic activity of EUGO, a reaction was performed using 1 mM 4-PG as a substrate in a Tris-HCl buffer (pH 8.0) containing 10  $\mu\text{M}$  EUGO and 10% DMSO at 37  $^{\circ}\text{C}$  for 8 h. HPLC analysis revealed that EUGO efficiently converted 4-PG into isoeugenol compared with the control group (Fig. 2E). Similarly, HPLC analysis confirmed that NOV1 catalyzed the conversion of isoeugenol to vanillin (Fig. 2E). These results suggested that EUGO and NOV1 are bioactive when expressed in BL21(DE3) separately.

On the other hand, leveraging the above hybrid display system, we constructed a vanillin bioconversion system by co-displaying EUGO and NOV1 on the surface

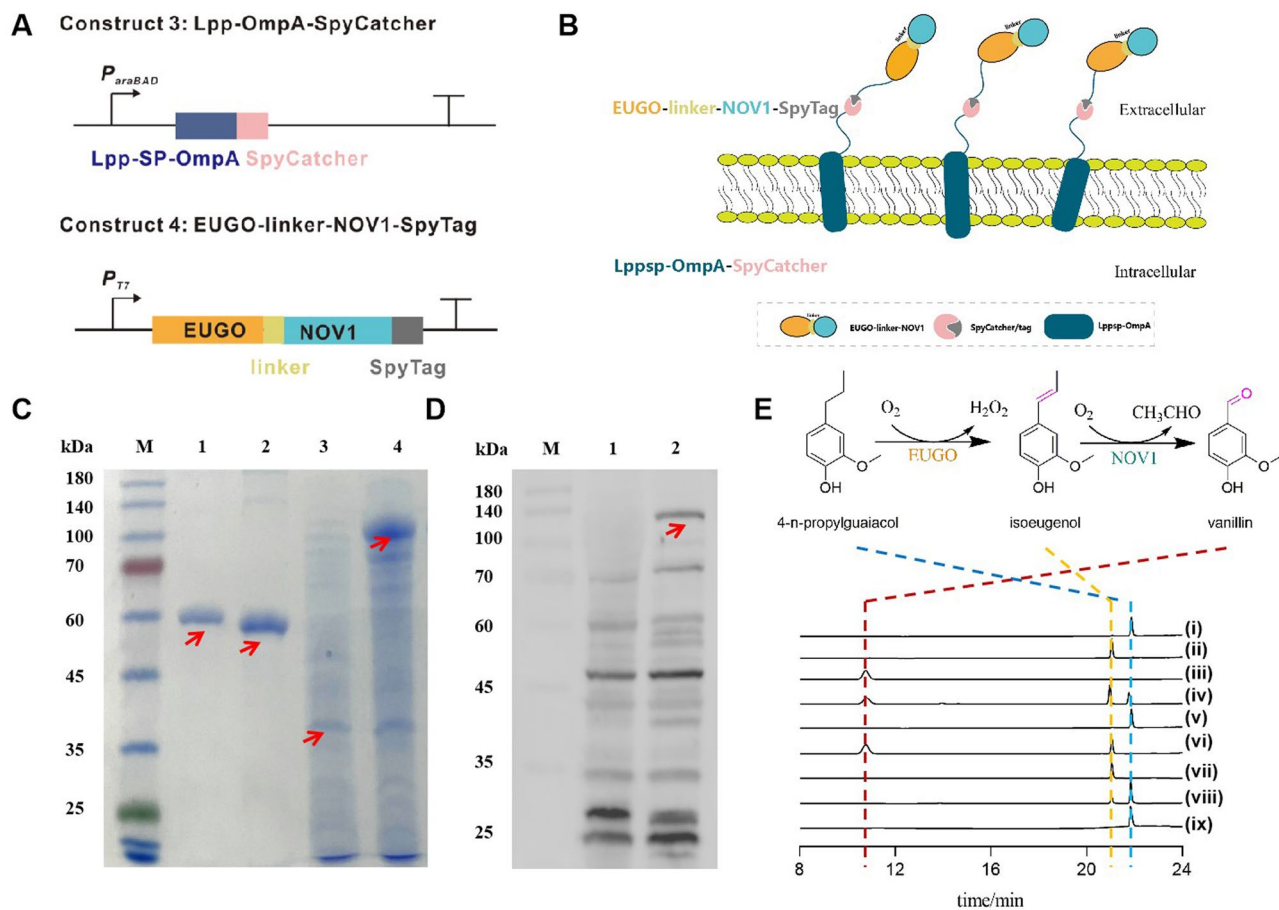


**Fig. 2** Construction of the EUGO and NOV1 co-display system for vanillin biosynthesis. **(A)** Design of constructs for the expression of EUGO and NOV1 and the covalent interaction between SpyCatcher and SpyTag. **(B)** Schematic diagram showing the assembly pattern of EUGO and NOV1. **(C)** SDS-PAGE analysis of the purified EUGO, NOV1, and their hybrid protein complex after assembly. Target protein bands are indicated by arrows. Lane M, protein molecular weight marker; Lane 1, the purified EUGO (57.7 kDa); Lane 2, the purified NOV1 (54.7 kDa); Lane 3, *E. coli* BL21(DE3) harboring pWJ003 (Lpp-OmpA-SpyCatcher (35.9 kDa)); Lane 4, *E. coli* BL21(DE3) harboring pWJ003 and pWJ004 (Lpp-OmpA-SpyCatcher-SpyTag-NOV1-linker-EUGO (147.9 kDa)); **(D)** Western blot analysis of the hybrid protein complex after assembly. Lane M, protein molecular weight marker; Lane 1, BL21 cell harboring pBAD24 (control); Lane 2, Lpp-OmpA-SpyCatcher-SpyTag-NOV1-linker-EUGO (147.9 kDa). **(E)** HPLC analysis of bioactivity of EUGO, NOV1 and the LOAS-ELNS. (i) 4-PG (standard); (ii) isoeugenol (standard); (iii) vanillin (standard); (iv) BL21 cells harboring pWJ003 and pWJ004; (v) BL21 cells harboring pBAD24 and pET28a (+); (vi) NOV1; (vii) boiled NOV1; (viii) EUGO; (ix) boiled EUGO

of *E. coli* BL21(DE3) cells. Similarly, we inserted the Lpp-OmpA-SpyCatcher fragment into pBAD24 and the EUGO-linker-NOV1-SpyTag fragment into pET28a (+) (Fig. 2A and B), resulting in plasmids pWJ003 and pWJ004, respectively. Subsequently, these two plasmids were co-transformed into *E. coli* BL21(DE3). Here, EUGO-linker-NOV1-SpyTag was designed as a His-tag-free protein, while the Lpp-OmpA-SpyCatcher module included a 6xHis-tag. When pWJ003 (containing the Lpp-OmpA-SpyCatcher module) and pWJ004 (containing the EUGO-linker-NOV1-SpyTag module) were co-transformed and induced, EUGO-linker-NOV1-SpyTag and Lpp-OmpA-SpyCatcher were expressed separately and formed the LOAS-ELNS complex via the interaction between SpyCatcher and SpyTag. Therefore, there is only one 6 X His-tag in the LOAS-ELNS complex. When

utilizing rabbit anti-6xHis tag as the primary antibody and HRP-conjugated goat anti-rabbit IgG as the secondary antibody for Western blot detection, the observed molecular weight of 147.9 kDa indicates the formation of the LOAS-ELNS complex. SDS-PAGE and western blot analysis showed that there existed a target protein band about 147.9 kDa (Fig. 2C and 2D). HPLC analysis revealed that LOAS-ELNS system can catalyze 4-PG into vanillin (Fig. 2E). In summary, we successfully constructed a hybrid vanillin bioconversion system by co-displaying EUGO and NOV1.

#### Optimization of the LOAS-ELNS surface display system

After the successful construction of the LOAS-ELNS surface display system, further optimization was conducted on the production conditions of this system. Initially, we

compared the growth curves of *E. coli* BL21(DE3), *E. coli* BL21(DE3) harboring pWJ001 and pWJ002, and *E. coli* BL21(DE3) harboring pWJ003 and pWJ004 and found that the three cells showed the same growth trend within 12 h (Fig. 3A). This result indicated that the LOAS-ELNS display system had no impact on cell growth within 12 h. To study the effect of cultivation temperature on LOAS-ELNS expression after induction, *E. coli* BL21(DE3) harboring pWJ003 and pWJ004 was induced at 18°C, 25°C, 30°C, and 37°C. The optimal expression temperature was determined to be 37°C based on the results of SDS-PAGE analysis (Figure S1). However, the cells expressing the enzyme at 37°C exhibited decreased activity, whereas the cells expressing the protein at 25°C demonstrated optimal activity (Fig. 3B). Thus, the optimal expression temperature for the LOAS-ELNS system in subsequent studies was set at 25°C.

#### Optimization the biosynthetic productivity of the LOAS-ELNS system

To optimize the reaction conditions of the LOAS-ELNS system, various parameters including temperatures, pH values, concentrations of DMSO, LOAS-ELNS cells, and 4-PG were systematically analyzed and compared to determine the most suitable reaction conditions.

Initially, enzymatic activities of LOAS-ELNS biosynthetic system at different temperatures were tested. The results demonstrated that the LOAS-ELNS display cells had the highest enzyme activity at 30°C, with the concentration of vanillin reaching 6.65 g/L and the conversion rate being about 44%. Further increase in temperature resulted in a decreased conversion rate and vanillin yield (Fig. 4A). Therefore, we determined that the optimal catalytic temperature was 30°C.

Then, different pH values were detected to optimize LOAS-ELNS biosynthetic system. When the

LOAS-ELNS biosynthetic system was tested under acidic conditions, the vanillin yield was found to be lower than 0.1 g/L. As the pH value increased from 6.0 to 11.0, the conversion rate at pH 8.0 was comparable to that at pH 10.0, with a final vanillin concentration reaching 7.16 g/L (Fig. 4B). To minimize cell lysis and considering the similarity between the conversion rates at pH 8.0 and pH 10.0, we proceeded with Tris-HCl buffer (50 mM, pH 8.0).

To test the amount of biocatalyst in the biosynthetic reaction, freshly prepared LOAS-ELNS cells were resuspended in Tris-HCl (50 mM, pH 8.0) and then added to the reaction system with final cell densities of 10, 20, 30, 40, and 50 g cww/L (cww, cell wet weight), respectively. When the cell density was 30 g cww/L, the yield of vanillin reached an optimal level of 7.52 g/L (Fig. 4C), and the conversion rate was about 76%.

Due to the poor water solubility of 4-PG, in order to increase the solubility of this substrate, we investigated the tolerance of the hybrid display system to different DMSO concentrations (0, 2.5%, 5%, 7.5%, and 10%). When the concentration of DMSO was 7.5% (v/v), the concentration of the final product vanillin reached the highest value 10.63 g/L (Fig. 4D). It is worth noting that compared with the conversion rate of 76% in Fig. 4C, the conversion rate in Fig. 4D is lower, but the vanillin concentration in Fig. 4D is increased, which is probably caused by the accumulation of intermediate isoeugenol.

The optimal substrate concentration facilitates the smooth progression of the reaction, as excessively high concentrations may inhibit enzyme activity, while insufficient concentrations fail to reach the maximum catalytic rate of enzymes. Therefore, we investigated the effect of the concentration of substrate 4-PG on the reaction. The peak enzyme activity was observed at 0.5 mM 4-PG (16.622 g/L), generating vanillin at a concentration

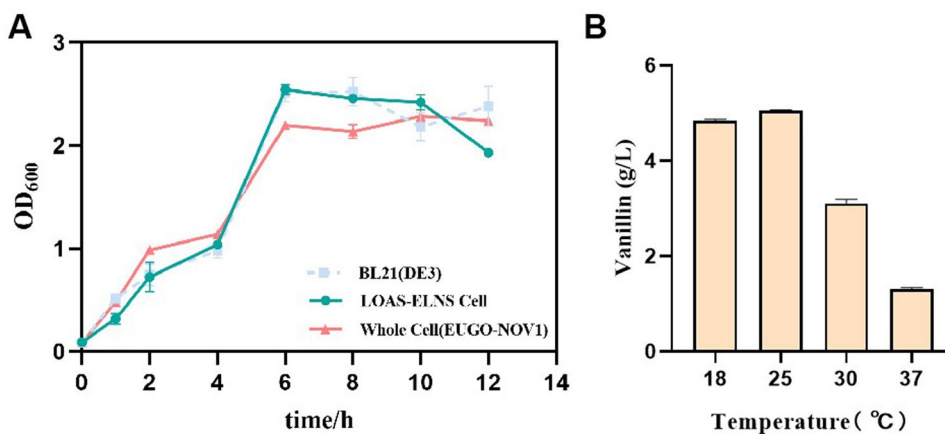


**Fig. 3** Optimization of the production conditions of LOAS-ELNS system. **(A)** The growth curve of *E. coli* BL21(DE3), *E. coli* BL21(DE3) harboring pWJ001 and pWJ002 and *E. coli* BL21(DE3) harboring pWJ003 and pWJ004; **(B)** The enzymatic activities of LOAS-ELNS display cells at different expression temperature were analyzed

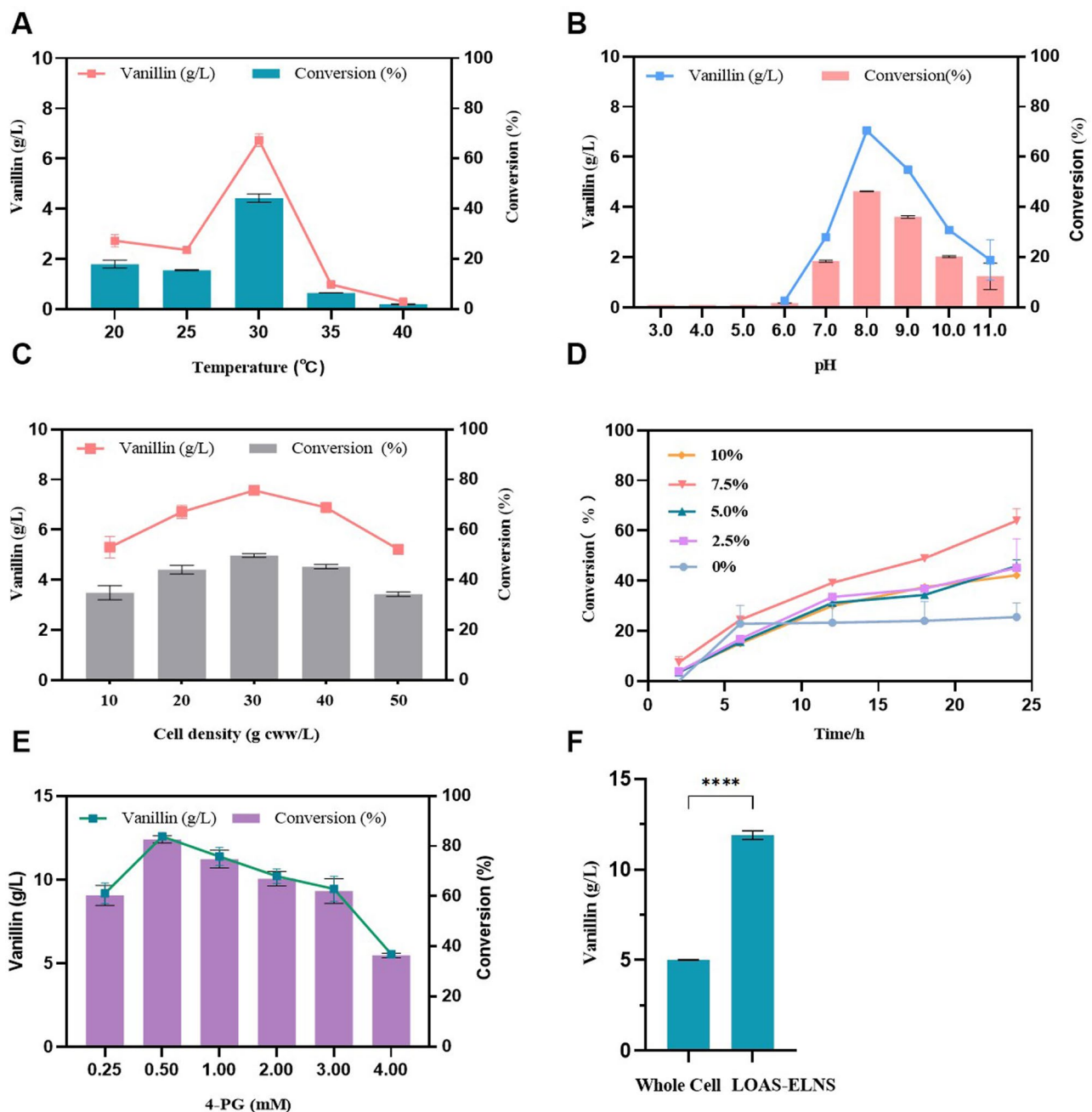


**Fig. 4** Optimization of the LOAS-ELNS biosynthetic system to improve the yield of vanillin and comparison of the catalytic activity of whole cells with that of LOAS-ELNS cells. **(A)** the enzymatic activities of LOAS-ELNS display cells under different reaction temperatures (20°C, 25°C, 30°C, 35°C, 40°C); **(B)** the enzymatic activities of LOAS-ELNS display cells under different pH values (pH 3.0–11.0); **(C)** the effect of cell density on the vanillin synthesis; **(D)** the enzymatic activities of LOAS-ELNS display cells under different DMSO concentration (v/v, 0%, 2.5%, 5.0%, 7.5%, 10.0%). **(E)** the enzymatic activities of LOAS-ELNS cells under different 4-PG concentrations. The yield of vanillin increased as the initial 4-PG concentration was raised from 0.25 to 0.5 mM (16.622 g/L), but it subsequently decreased when the 4-PG concentration was further increased from 0.5 to 4.0 mM. The highest production (12.58 g/L) and conversion rate were obtained with 0.5 mM 4-PG (16.622 g/L). The mixtures were incubated at 30°C, pH 8.0, with the cell density of 30 g cww/L, 0.5 mM (16.622 g/L) 4-PG and 7.5% DMSO. **(F)** Comparison of vanillin yield between whole cell and LOAS-ELNS systems. The values are presented as means with error bars indicating the standard deviation based on at least three independent tests. \*\*\*\* $P < 0.0001$ . Each experiment was conducted in triplicate

of 12.58 g/L, which represents a 1.5-fold improvement compared to the yield achieved with 0.25 mM 4-PG (Fig. 4E). Therefore, 0.5 mM 4-PG (16.622 g/L) was chosen as the substrate concentration for further reactions.

Under optimal reaction conditions, we compared the catalytic activity of LOAS-ELNS cells with that of whole cells and determined the optimal temperature and pH for purified EUGO and NOV1 related to whole cells (Figure

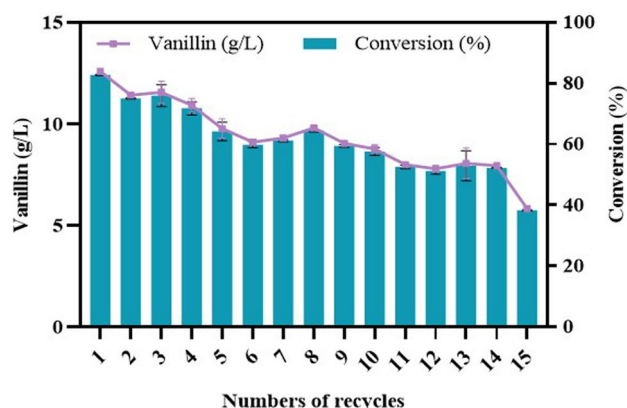


**Fig. 5** Reused times of the LOAS-ELNS display cells. Following each enzymatic reaction, the cells were subjected to centrifugation and washed with the assay buffer. Subsequently, the activities of LOAS-ELNS display cells were promptly reassessed to evaluate their repetitive usage. Each experiment was conducted in triplicate

S2). Compared to the whole cells harboring pWJ001 and pWJ002, the LOAS-ELNS biosynthetic cells exhibited a 2.5-fold increase in vanillin yield (Fig. 4F). The Whole cell catalysis involves a two-step reaction process: the conversion of 4-PG to isoeugenol and subsequently from isoeugenol to vanillin. The final conversion rate of 4-PG to vanillin in this process was about 30%. In contrast, in the LOAS-ELNS system, the ultimate conversion rate of 4-PG to vanillin reached 83.4%, with a yield of 12.58 g/L. This result was partly attributed to the spatial proximity of EUGO and NOV1 and removed the barrier for substrate transportation. In summary, the LOAS-ELNS display system produced 12.58 g/L vanillin with the cell density of 30 g cww/L at 30°C, pH 8.0, 0.5 mM (16.622 g/L) 4-PG, and 7.5% DMSO.

#### Evaluation of the reusability of the LOAS-ELNS display system

The reuse and regeneration of catalysts is an effective strategy for cost reduction in catalytic processes. However, achieving efficient separation and recovery of soluble enzymes in catalytic reactions poses challenges due to their uniform distribution and mixing within the reaction system, which hinders their recycling. In contrast, whole-cell catalysts can be easily reused after a reaction through various methods such as centrifugation, filtration, etc., due to their distinctive cell structure characteristics. Moreover, whole-cell catalytic systems exhibit higher enzyme activity within the same catalytic time and number of uses, thereby further enhancing their attractiveness for industrial applications. In order to further explore the reusability of LOAS-ELNS catalysts, 15 rounds of LOAS-ELNS display cell enzymatic activity were investigated experimentally. The LOAS-ELNS display cells were successfully reused three times under optimized reaction conditions, with their activities

remaining above 92% of their initial activity. Additionally, the LOAS-ELNS display cells demonstrated successful reusability for ten cycles under optimized reaction conditions while maintaining their activities above 70% of their original levels (Fig. 5). The relative conversion rate for cells reused more than 15 times fell below 50%, which can be partially attributed to the formation of hydrogen peroxide and other detrimental byproducts during the reaction, adversely affecting enzyme activity. These results indicated that the LOAS-ELNS display system showed good reusability.

In this study, the LOAS-ELNS cells function as a source of purified enzyme, thereby eliminating the need for separate EUGO and NOV1 purification processes. Compared with whole-cell catalysis that relies on intracellular enzymes, this approach removes the requirement for transmembrane transport of substrates and products [23]. Especially, the SpyCatcher/SpyTag system, which often functions as multienzyme scaffolds, can enhance biocatalytic efficiency, avoid potential cellular toxicity, enable direct catalysis, provide modularity, integrate enzymes from diverse sources, and demonstrate the potential to design *de novo* synthetic cascades [36]. After the integration of the SpyCatcher/SpyTag, the molecular weight of the passenger protein displayed by Lpp-OmpA was not limited as previously reported. Additionally, we successfully demonstrated the bioactive EUGO-linker-NOV1 (147.9 kDa). In our initial experiment, the absence of SpyCatcher/SpyTag resulted in the failure to display EUGO-linker-NOV1, thereby confirming the necessity of the SpyCatcher/SpyTag system for the LOAS-ELNS display system.

Here, we utilized 4-n-propylguaiacol (4-PG), obtained from the decomposition of lignin, as the substrate for vanillin bioconversion. As one of the most abundant natural sources, lignin can be decomposed into low-molecular-weight oligomers and, importantly, phenolic monomers with high yield and selectivity (21–50%, with 27.1% being 4-PG) using the reductive catalytic fractionation (RCF) method. Despite the high proportion of 4-PG among the hydrolysis products of lignin, research on its applications remains relatively limited [7]. When EUGO and NOV1 were co-displayed as a complex to convert 4-PG to vanillin, the yield reached 83.4%, 12.58 g/L, and the LOAS-ELNS cells could be reused for at least 10 cycles. Marić et al. reported a one-pot whole-cell cascade process for the synthesis of vanillin from 4-PG utilizing two strains of *E. coli*. The dual-enzyme catalysis system, which expresses PROGO and NOV1F respectively, achieved a vanillin yield of 66% from 4-PG. Furthermore, the researchers investigated the utilization of lignin oil and spruce wood as raw materials, achieving yields of 18% and 3%, respectively. Compared to their work, both EUGO and NOV1 exhibit lower catalytic efficiency than

PROGO and NOV1F when using 4-PG and isoeugenol as substrates, respectively [7]. However, our final yield reached 83.4%, which can be attributed to the utilization of a surface display system. This approach eliminates the need for substrate and product transport across the cell membrane. Furthermore, this improvement is probably attributed to the influence of spatial proximity, which effectively hinders the diffusion of intermediates within the reaction mixture, as demonstrated in numerous previous studies [25]. Nonetheless, their whole-cell biocatalysis involves a two-step cascade, which may restrict its subsequent reuse.

EUGO is a promising enzyme for industrial-scale production of “natural” vanillin, which is underpinned by its exceptional expression in *E. coli*, its ability to utilize various 4-substituted phenols as substrates, stability and activity over a wide pH range, and remarkable solvent tolerance [19]. García-Bofill et al. utilized EUGO (eugenol oxidase) for the bioproduction of vanillin through the oxidation of vanillyl alcohol, achieving a yield of 2.9 g/L/h [18]. Furthermore, they demonstrated that EUGO can be efficiently immobilized on various supports, including MANA–agarose, Epoxy–agarose, and Pololite 8204 F, enabling several recycles while maintaining high stability. In a subsequent study, by optimizing the reaction and immobilization conditions, they significantly increased the vanillin yield to 9.9 g/L/h. More importantly, the use of immobilized EUGO allowed for up to 18 reuses of the biocatalyst, enhancing its efficiency more than 12-fold and consequently reducing associated biocatalyst costs [19]. Compared to their work, we successfully displayed EUGO-linker-NOV1 on the surface of *E. coli*, achieving an efficient two-step enzyme cascade conversion from 4-PG to vanillin. Furthermore, the LOAS-ELNS cells can be reused at least 10 times while maintaining a yield above 70% relative to the initial run. These advantages provide the basis for industrial applications in the future.

NOV1, a non-heme iron-dependent dioxygenase enzyme, catalyzes the coenzyme-independent oxidation of isoeugenol to vanillin. This enzymatic process holds significant biotechnological potential for the comprehensive valorization of lignin as a sustainable feedstock for the production of bio-based chemicals, polymers, and materials. A recent study employing computer-guided mutagenesis of NOV1 demonstrated that the catalytic efficiency ( $K_{cat}/K_m$ ) of the S235F mutant was up to 4-fold higher compared to NOV1. In whole-cell biocatalysis experiments utilizing the S235F mutant for the conversion of isoeugenol to vanillin, the yield approached 100% [35].

In future studies, we will focus on several aspects to improve the LOAS-ELNS system. Specifically, we aim to engineer enzymes to improve their catalytic efficiency and selectivity, immobilize LOAS-ELNS cells to increase

their reusability, and optimize the enzyme cascade process through the use of multi-enzyme scaffolds [37, 38]. Notably, incorporating catalase into the surface display system can effectively decompose hydrogen peroxide generated during the reaction, thereby extending the lifespan of the enzymes.

## Conclusion

In this study, we constructed a hybrid biosynthetic system by combining the endogenous anchoring motif Lpp-OmpA of *E. coli* with the SpyTag/SpyCatcher protein pair system to display the EUGO and NOV1 complex for the production of vanillin. The biocatalytic cascade of vanillin production used lignin-derived 4-n-propylguaiacol (4-PG) as a starting material. The catalytic conditions of LOAS-ELNS display cells were optimized concerning temperature, pH values, the amounts of cells, the concentration of 4-PG and DMSO. Under optimal reaction conditions, the vanillin yield reached 12.58 g/L, which was 2.5-fold higher than that of whole-cell catalytic system. Our approach provides a foundation for the sustainable production of bio-based vanillin, facilitating further advancements in this field.

## Materials and methods

### Bacterial strains, plasmids, gene sources and reagents

*E. coli* DH5 $\alpha$  and BL21(DE3) serve as molecular cloning hosts and expression hosts, respectively. pET28a (+) and pBAD24 were used as expression vectors. All plasmids used in this study were listed in Table S1. EUGO (GenBank: ABG95085.1) and NOV1 (GenBank: ABD25247.1) were synthesized by Sangon Biotech (Shanghai, China). The genes for *lpp-ompA*, *spyttag/spycatcher*, *sfgfp* and *mcherry* were amplified from plasmids stored in our lab [39].

Bacterial genomic DNA extraction kit, plasmid purification kit, and gel purification kit were purchased from Shanghai GJ Bioengineering Co., Ltd., while 2 $\times$ Taq Plus PCR MasterMix was purchased from Vazyme Biotech Co., Ltd. The SDS-PAGE gel kit was purchased from Shanghai Epizyme Biomedical Technology Co., Ltd., and the protein molecular weight markers were purchased from Hunan Aikrui Biological Engineering Co., Ltd. All other analytical grade chemical reagents were purchased from Shanghai Aladdin Biochemical Technology Co., Ltd. All restriction endonucleases and homologous recombination enzymes were provided by Yeasen Biotechnology (Shanghai) Co., Ltd., and the primers (Table S2) and gene sequencing used in the experiment were synthesized by Beijing Qingke Biotechnology Co., Ltd.

### Plasmid construction

In general, the plasmids were derived from two sources: pWJ001 and pWJ002 was chemically synthesized to

express EUGO and NOV1, respectively; the other plasmids were constructed involved PCR amplification, overlapping PCR, and homologous recombination techniques, etc.

The fragments of *lpp-ompA*, *spycatcher* and *sfgfp* were amplified from plasmids pET28a (+)-LOA-SC and pET28a(+)-GFP using three primer pairs: OMPA-F/OMPA-R, Spy-F/Spy-R and SFGFP-F/SFGFP-R, respectively. Then, *mcherry-spytag* was amplified from pET28a (+)-mCherry using primers mcherrytag-F1, mcherrytag-F2, and mcherrytag-R. Subsequently, the fragments of *lpp-ompA*, *sfgfp*, and *spycatcher* were ligated into the XhoI and HindIII linearized pBAD24 through homologous recombination. Similarly, the fragment of *mcherrytag* was inserted to the NdeI and EcoRI linearized pET-28a (+) resulting in recombinant plasmids pBAD24-OmpA-sfGFP-SpyCatcher (pWJ005) and pET-28a (+)-mCherry-SpyTag (pWJ006). Finally, the confirmation of pWJ005 and pWJ006 was achieved through sequencing.

Using pET28a (+)-LOA-SC as the template, the fragment of *lpp-ompA* was amplified with primers OMPA-F2/OMPA-R2. The fragment of *spycatcher* was amplified using primers Spy-F2/Spy-R2, and the fragments of *lpp-ompA* and *spycatcher* were inserted into the XhoI and HindIII linearized pBAD24 by homologous recombination. The plasmid pBAD24-Lpp-OmpA-SpyCatcher(pWJ003) was obtained. The fragment of *nov1-spytag* was amplified using primers NOV1-TAG-F, NOV1-TAG-R1, and NOV1-TAG-R2 with pET28a (+)-NOV1 (pWJ002) as the template. The fragment of *eugo-linker* was amplified by primers EUGO-F and EUGO-R with pBAD24-EUGO (pWJ001) as the template. The plasmid pET28a (+)-EUGO-linker-NOV1-SpyTag (pWJ004) was obtained by homologous recombination of fragments NOV1-SpyTag and EUGO-linker into NdeI and EcoRI linearized pET28a (+). Sequencing confirmed that the plasmids pWJ003 and pWJ004 were constructed correctly.

#### Cell surface display

The pWJ003 and pWJ004 (or pWJ005/pWJ006) were transformed into *E. coli* BL21(DE3) competent cells sequentially, and the monoclonal was selected and cultured overnight at 220 rpm and 37°C. Subsequently, overnight cultures were inoculated at 1:100 and cultivated at fresh LB broth (10 g/L tryptone, 5 g/L yeast extract, and 10 g/L NaCl) with 100 µg/mL Ampicillin and 50 µg/mL Kanamycin at 37°C. When OD<sub>600</sub> reached 0.6–0.8, the cells were induced with the final concentration of 1 mM L-arabinose and 0.4 mM isopropyl-β-D-1-thiogalactopyranoside (IPTG) and cultivated at 25°C for 16 h. The cells were then collected by centrifugation at 5,000 rpm for 10 min at 4°C and washed twice with

100 mM phosphate buffer (pH 7.4). The cell pellets were resuspended and standardized to OD<sub>600</sub> of 2.5 (about 30 g cww/L) with the corresponding buffers for the following experiments.

#### Protein expression and purification

To express EUGO and NOV1, plasmids pWJ001 or pWJ002 were transformed into *E. coli* BL21(DE3). The strain harboring the relevant plasmid was cultured for protein expression and purification. Seed culture was cultivated overnight at 37°C in LB broth with appropriate antibiotics (100 µg/mL ampicillin or 50 µg/mL kanamycin). Then, the overnight cultures were inoculated at 1:100 and cultured in fresh LB broth supplemented with ampicillin (100 µg/mL) or kanamycin (50 µg/mL) at 37°C until the OD<sub>600</sub> reached 0.6–0.8. The cells were induced with the final concentration of 1 mM L-arabinose or 0.4 mM IPTG at 25°C for 16 h. After centrifugation at 5,000 rpm at 4°C for 10 min, cell pellets were resuspended using lysis buffer (Buffer A: 50 mM Tris-HCl, 300 mM NaCl, 10 mM imidazole, 10% glycerol, and pH 8.0) and subsequently lysed through sonication (50% amplitude, 7 s on and 3 s off for a total of 30 min). After centrifugation at 12,000 rpm for 30 min at 4°C, the supernatant was transferred to a new centrifuge tube for another 30 min, and then the supernatant was collected. The supernatant was loaded to Ni-NTA His-Tag purification agarose after filtration through 0.22 µm filter membrane (Merck). Then, the Ni-NTA columns were sequentially eluted with buffer A containing 10 mM, 50 mM, 100 mM, and 500 mM of imidazole to obtain target proteins. The elution samples containing the target proteins were desalted using a desalting buffer (50 mM Tris-HCl, 50 mM NaCl, 10% glycerol, and pH 8.0) and concentrated by centrifugation at 3,500 rpm and 4°C using Amicon Ultra-15 centrifugal filters (10 kDa cutoff, Merck). After determining the concentrations of purified proteins, they were frozen in liquid nitrogen and stored at -80°C for further use.

#### Western blot analysis

Protein samples (50 µL) were mixed with 5 µL of a 5×loading buffer and denatured in boiling water for 15 min. Then, the denatured samples were analyzed by SDS-PAGE and transferred onto a PVDF membrane for sequential incubation with anti-His antibodies. Finally, the target protein band on the PVDF membrane was visualized using Super ECL A and Super ECL B reagent (Super ECL A: Super ECL B = 1:1). (Wuhan Pumokey Biotechnology Co., Ltd.)

#### Confocal laser scanning microscopy

Harvest the cell pellets of *E. coli* BL21(DE3) containing pWJ005 and pWJ006 (1 mL of LB broth) at an OD<sub>600</sub> reached 2.5 by centrifugation (6,000 rpm, 5 min, 4°C).

Then, resuspend the cell pellets in 5 mL of phosphate buffered saline (PBS, pH 7.2–7.4). 5  $\mu$ L of suspension samples were loaded onto a microscope slip and observed with a Confocal Laser Scanning Microscopy for fluorescence imaging.

### Enzymatic activity assays

The enzymatic activity of EUGO was conducted in 1.5 mL Eppendorf tubes. Each reaction (500  $\mu$ L) contained 1 mM 4-PG, 10  $\mu$ M EUGO and 10% (v/v) DMSO, and was performed at 37°C for 8 h in 50 mM Tris-HCl buffer (pH 8.0). The NOV1 reaction system (500  $\mu$ L) containing 1 mM isoeugenol, 5  $\mu$ M NOV1 and 10% (v/v) DMSO was conducted at 30°C for 8 h in 50 mM Tris-HCl buffer (pH 8.0). The analysis of LOAS-ELNS catalytic activity was carried out at 30°C for 24 h in 50 mM Tris-HCl buffer (pH 8.0) containing 0.5 mM 4-PG (16.622 g/L), 7.5% (v/v) DMSO and resuspended cell pellets (final concentration 30 g cww/L, OD<sub>600</sub>  $\approx$  2.5). All reactions were added with an equal volume of ethanol and thoroughly mixed. Subsequently, the mixture was centrifuged at 12,000 rpm for 15 min and filtered using a 0.22  $\mu$ m filter membrane before being transferred into sample bottles. The conversion was defined as the ratio of the actual yield of the product to the theoretical yield, based on the initial quantity of 4-PG.

$$\%Conversion = \frac{\text{actual yield}}{\text{theoretical yield}} \times 100\%$$

### Analytical methods

Vanillin and isoeugenol were detected by Agilent 1260 High performance liquid chromatography (HPLC) on Agilent C18 column ZORBAX SB-C18 5  $\mu$ m (150 mm  $\times$  4.6 mm, 5  $\mu$ m). The mobile phase consisted of 0.1% acetic acid water (buffer A)-methanol (buffer B)-with a flow rate of 0.5 mL/min through a linear gradient elution. The gradient elution conditions involve maintaining a 35% methanol elution for 7 min, followed by a gradual transition from 35 to 100% methanol over 15 min. Finally, the methanol concentration decreases back to 35% over another 7 min. The detection wavelength of vanillin is 280 nm. The amount of vanillin is quantified by drawing a series of standard curve concentrations (25, 50, 100, 200, 500 mg/L). All samples were tested three times.

### Supplementary Information

The online version contains supplementary material available at <https://doi.org/10.1186/s12934-025-02680-6>.

Supplementary Material 1

### Author contributions

J.W. conceived and designed the experiments, analyzed the data, supervised the work, and wrote and confirmed the manuscript. Y.T. performed the experiments, analyzed the data, and confirmed the manuscript. Y.Y. and M.N. reviewed and edited the manuscript. All authors read and approved the final manuscript.

### Funding

This work was supported by the National Key Research and Development Program of China (No. 2023YFA0914200).

### Data availability

No datasets were generated or analysed during the current study.

### Declarations

#### Competing interests

The authors declare no competing interests.

Received: 20 December 2024 / Accepted: 19 February 2025

Published online: 07 March 2025

### References

- Xu LX, Liaqat F, Sun JZ, Khazi MI, Xie RR, Zhu DC. Advances in the Vanillin synthesis and biotransformation: A review. *Renew Sust Energy Rev*. 2024.
- Banerjee G, Chattopadhyay P. Vanillin biotechnology: the perspectives and future. *J Sci Food Agric*. 2019;99:499–506.
- Liu Y, Sun L, Huo YX, Guo S. Strategies for improving the production of bio-based Vanillin. *Microb Cell Fact*. 2023;22:147.
- Amr K, Rasheed DM, Khachila M, Farag MA. Production, extraction, and authentication of natural and non-natural Vanillin. A comprehensive review and economic future biotechnology perspectives. *Food Chem*. 2025;466:142249.
- Ma Q, Liu L, Zhao S, Huang Z, Li C, Jiang S, Li Q, Gu P. Biosynthesis of Vanillin by different microorganisms: a review. *World J Microbiol Biotechnol*. 2022;38:40.
- Mostafa HS, Hashem MM. Lactic acid bacteria as a tool for Biovanillin production: A review. *Biotechnol Bioeng*. 2023;120:903–16.
- Marić I, Guo YM, Fürst MJL, Aelst KV, Bosch SVD, Simone MD, Martins LO, Sels BF, Fraaije MW. A One-Pot, Whole-Cell biocatalysis approach for Vanillin production using lignin oil. *Adv Synth Catal*. 2023;365:3987–95.
- Zheng R, Chen Q, Yang Q, Gong T, Hu CY, Meng Y. Engineering a carotenoid cleavage Oxygenase for Coenzyme-Free synthesis of Vanillin from ferulic acid. *J Agric Food Chem*. 2024;72:12209–18.
- Valério R, Bernardino ARS, Torres CAV, Brazinha C, Tavares ML, Crespo JG, Reis MAM. Feeding strategies to optimize Vanillin production by *Amycolatopsis* Sp. ATCC 39116. *Bioprocess Biosyst Eng*. 2021;44:737–47.
- Suresh B, Ravishankar GA. Methyl jasmonate modulated biotransformation of phenylpropanoids to Vanillin related metabolites using *Capsicum frutescens* root cultures. *Plant Physiol Biochem*. 2005;43:125–31.
- Sharma A, Sahu S, Sharma S, Singh G, Arya SK. Valorization of agro-industrial wastes into Vanillin: a sustainable and bio-economical step towards the Indigenous production of flavors. *Biocatal Agric Biotechnol*. 2023;54.
- Gao J, Zuo Y, Xiao F, Wang YL, Li DF, Xu JH, Ye CF, Feng LJ, Jiang LJ, Liu TF, Gao D, Ma B, Huang L, Xu ZN, Lian JZ. Biosynthesis of catharanthine in engineered *pichia pastoris*. *Nat Synth*. 2023;2.
- Cai T, Sun H, Qiao J, Zhu L, Zhang F, Zhang J, Tang Z, Wei X, Yang J, Yuan Q, et al. Cell-free chemoenzymatic starch synthesis from carbon dioxide. *Science*. 2021;373:1523–7.
- Li K, Frost JW. Synthesis of Vanillin from glucose. *J Am Chem Soc*. 1998;120:10545–6.
- Martão GA, Cãlinoi LF, Vodnar DC. Bio-vanillin: towards a sustainable industrial production. *Trends Food Sci Technol*. 2021;109:579–92.
- Chakraborty D, Kaur B, Obulisamy K, Selvam A, Wong JWC. Agrowaste to Vanillin conversion by a natural *Pediococcus acidilactici* strain BD16. *Environ Technol*. 2017;38:1823–34.
- Hansen EH, Moller BL, Kock GR, Bunner CM, Kristensen C, Jensen OR, Okkels FT, Olsen CE, Motawia MS, Hansen J. *De Novo* biosynthesis of Vanillin in

- fission yeast (*Schizosaccharomyces pombe*) and Baker's yeast (*Saccharomyces cerevisiae*). *Appl Environ Microbiol.* 2009;75:2765–74.
18. Garcia-Bofill M, Sutton PW, Guillén M, Alvaro G. Enzymatic synthesis of Vanillin catalysed by an Eugenol oxidase. *Appl Catal A-Gen.* 2019;582.
  19. Garcia-Bofill M, Sutton PW, Straatman H, Brummund J, Schürmann M, Guillén M, Alvaro G. Biocatalytic synthesis of Vanillin by an immobilised Eugenol oxidase: high biocatalyst yield by enzyme recycling. *Appl Catal A-Gen.* 2021;610.
  20. Kim HG, Jang Y, Shin JS. One-Pot production of Vanillin from capsaicinoids through a retrosynthetic enzyme cascade. *Adv Synth Catal.* 2024;366:1877–87.
  21. Liu Y, Huang S, Liu WQ, Ba F, Liu Y, Ling S, Li J. An *in vitro* hybrid biocatalytic system enabled by a combination of Surface-Displayed, purified, and Cell-Free expressed enzymes. *ACS Synth Biol.* 2024;13:1434–41.
  22. Ye M, Ye Y, Du Z, Chen G. Cell-surface engineering of yeasts for whole-cell biocatalysts. *Bioprocess Biosyst Eng.* 2021;44:1003–19.
  23. Schuurmann J, Quehl P, Festel G, Jose J. Bacterial whole-cell biocatalysts by surface display of enzymes: toward industrial application. *Appl Microbiol Biotechnol.* 2014;98:8031–46.
  24. Gallus S, Peschke T, Paulsen M, Burgahn T, Niemeyer CM, Rabe KS. Surface display of complex enzymes by *in situ* SpyCatcher-SpyTag interaction. *ChemBioChem.* 2020;21:2126–31.
  25. Qiu XY, Xie SS, Min L, Wu XM, Zhu LY, Zhu L. Spatial organization of enzymes to enhance synthetic pathways in microbial chassis: a systematic review. *Microb Cell Fact.* 2018;17:120.
  26. Georgiou G, Stephens DL, Stathopoulos C, Poetschke HL, Mendenhall J, Earhart CF. Display of beta-lactamase on the *Escherichia coli* surface: outer membrane phenotypes conferred by Lpp'-OmpA'-beta-lactamase fusions. *Protein Eng.* 1996;9:239–47.
  27. Francisco JA, Earhart CF, Georgiou G. Transport and anchoring of beta-lactamase to the external surface of *Escherichia coli*. *Proc Natl Acad Sci U S A.* 1992;89:2713–7.
  28. Richins RD, Kaneva I, Mulchandani A, Chen W. Biodegradation of organophosphorus pesticides by surface-expressed organophosphorus hydrolase. *Nat Biotechnol.* 1997;15:984–7.
  29. Wan HM, Chang BY, Lin SC. Anchorage of cyclodextrin glucanotransferase on the outer membrane of *Escherichia coli*. *Biotechnol Bioeng.* 2002;79:457–64.
  30. Fan R, Aranko AS. Catcher/Tag toolbox: biomolecular Click-Reactions for protein engineering beyond genetics. *ChemBioChem.* 2024;25:e202300600.
  31. McAndrew RP, Sathitsuksanoh N, Mbughuni MM, Heins RA, Pereira JH, George A, Sale KL, Fox BG, Simmons BA, Adams PD. Structure and mechanism of NOV1, a resveratrol-cleaving dioxygenase. *Proc Natl Acad Sci U S A.* 2016;113:14324–9.
  32. Nguyen QT, Gonzalo GD, Binda C, Rioz-Martinez A, Mattevi A, Fraaije MW. Biocatalytic properties and structural analysis of Eugenol oxidase from *Rhodococcus jostii* RHA1: A versatile oxidative biocatalyst. *ChemBioChem.* 2016;17:1359–66.
  33. Eggerichs DZK, Tischler D. Large scale production of Vanillin using an Eugenol oxidase from *Nocardioides* sp. YR527. *Mol Catal.* 2023;546.
  34. Guo Y, Alvigini L, Trajkovic M, Alonso-Cotchico L, Monza E, Savino S, Maric I, Mattevi A, Fraaije MW. Structure- and computational-aided engineering of an oxidase to produce isoeugenol from a lignin-derived compound. *Nat Commun.* 2022;13:7195.
  35. Simone MD, Alvigini L, Alonso-Cotchico L, Brissos V, Caroli J, Lucas MF, Monza E, Melo EP, Mattevi A, Martins LO. Rationally guided improvement of NOV1 dioxygenase for the conversion of Lignin-Derived isoeugenol to Vanillin. *Biochemistry.* 2023;62:419–28.
  36. Ellis GA, Klein WP, Lasarte-Aragonés G, Thakur M, Walper SA, Medintz IL. Artificial multienzyme scaffolds: pursuing *in vitro* substrate channeling with an overview of current progress. *ACS Catal.* 2019;9:10812–69.
  37. Hwang ET, Lee S. Multienzymatic cascade reactions via enzyme complex by immobilization. *ACS Catal.* 2019;9:4402–25.
  38. Maghraby YR, El-Shabasy RM, Ibrahim AH, Azzazy HME. Enzyme immobilization technologies and industrial applications. *ACS Omega.* 2023;8:5184–96.
  39. Wo J, Lv ZY, Sun JN, Tang H, Qi N, Ye BC. Engineering probiotic-derived outer membrane vesicles as functional vaccine carriers to enhance immunity against SARS-CoV-2. *iScience.* 2023;26:105772.

## Publisher's note

Springer Nature remains neutral with regard to jurisdictional claims in published maps and institutional affiliations.